Crystal structure and Raman spectroscopic studies of OH stretching vibrations in Zn-rich fluor-elbaite

Adam Pieczka[1,*,†], Andreas Ertl[2], Bożena Gołębiowska[1], Piotr Jeleń[3], Jakub Kotowski[4], Krzysztof Nejbert[4], Marcin Stachowicz[4], and Gerald Giester[2]

[1]Department of Mineralogy, Petrography and Geochemistry, AGH University of Science and Technology, Mickiewicza 30, 30-059 Kraków, Poland
[2]Institut für Mineralogie und Kristallographie, Geozentrum, Universität Wien, Althanstrasse 14, 1090 Wien, Austria
[3]Faculty of Materials Science and Ceramics, AGH University of Science and Technology, Mickiewicza 30, 30-059 Kraków, Poland
[4]Faculty of Geology, Institute of Geochemistry, Mineralogy and Petrology, University of Warsaw, 02-089 Warszawa, Żwirki and Wigury 93, Poland

Abstract

Zinc-rich fluor-elbaite from Piława Górna, Poland, was studied by electron microprobe (EPMA), single-crystal X-ray diffraction (SREF), and Raman spectroscopy (RS) to check the possibility of the application of RS to draw crystal-chemical conclusions for Al-rich and Li-bearing tourmalines on basis of the O–H stretching vibrations in the spectral range 3400–3800 cm^{-1}. This tourmaline, forming a thin metasomatic zone around gahnite, features varying compositions with a ZnO content reaching in the studied fragment of 5.70(12) wt%. The crystal structure of this Zn-rich fluor-elbaite [$a = 15.921(1)$, $c = 7.127(1)$ Å] was refined with a $R1$ value of 1.67%. Its formula was determined on the basis of electron-microprobe and structure refinement as $^X(Na_{0.84}\square_{0.14}Ca_{0.01})_{\Sigma1.00}{}^Y(Al_{1.06}Li_{0.84}Zn_{0.69}Fe^{2+}_{0.32}Mn_{0.09})_{\Sigma3.00}{}^ZAl_6(BO_3)_3(^TSi_6O_{18})^V(OH)_3{}^W(F_{0.65}OH_{0.26}O_{0.09})$. The deconvolution of the O–H stretching vibration bands, performed by fitting of an input model of component bands with Gaussian function shapes for the empirical spectrum, indicates that each of the three maxima assigned for ^VOH bonded to $^YAl^{3+}$, Y^{2+}, and $^YLi^+$ and with the total integral intensity of at least 75% of the total OH content could be resolved into 1 to 3 bands, depending on the X-site occupation (vacancies, Na^+, and Ca^{2+}). The deconvolution indicates further that several low intense bands of ^WO–H modes above a Raman shift of 3600 cm^{-1}, totally reaching ≤25%, are dependent on the occupation of triplets of YYY cations bonded to the hydroxyl. These ^WO–H modes are also influenced by the X-site occupation. Due to ordering of all octahedral cations (except Al) at the Y site and a complete occupation of the Z site by Al and the V site by OH, it seems possible to evaluate the Li and OH contents in a Al-rich and Li-bearing tourmaline directly from the Raman spectrum. By using the ratio $^{VOH}I_{YAlZAlZAl}/(^{VOH}I_{YZZ} + {}^{WOH}I_{YYY})$ as evaluated from RS, corresponding to the ratio $^YAl/^{V+W}OH$ in the crystal, the formula of the Zn-rich fluor-elbaite can be calculated as $^X(Na_{0.85}\square_{0.14}Ca_{0.01})_{\Sigma1.00}{}^Y(Al_{1.11}Y^{2+}_{1.11}Li_{0.78})_{\Sigma3.00}{}^ZAl_6(BO_3)_3(Si_6O_{18})(OH)_3(F_{0.65}OH_{0.13}O_{0.22})$, where $Y^{2+} = Zn + Fe + Mn$. The formula, determined only on basis of EPMA and deconvolution of RS in the O–H stretching bands, corresponds very well (≤1 SD range of EPMA) to the formula determined on basis of EPMA and SREF. This result implicates that the O–H stretching vibrations, measured by Raman spectroscopy, could be applied for Al-rich and Li-bearing tourmalines as a useful tool for providing additional information for determining the crystal-chemical formula. It is also very helpful when crystal structural data are not available.

Keywords: Zn-rich fluor-elbaite, structure refinement, Raman spectroscopy, OH stretching vibrations, lithium content, hydroxyl content; Lithium, Beryllium, and Boron: Quintessentially Crustal

Introduction

The tourmaline supergroup comprises complex borosilicates that are found as accessory minerals in a wide variety of igneous, metamorphic, and sedimentary rocks due to their stability over a wide range in pressure, temperature, and composition (Van Hinsberg et al. 2011). The generalized formula of tourmaline-supergroup minerals is $XY_3Z_6(T_6O_{18})(BO_3)_3V_3W$, where X, Y, Z, T, B, V (= O3), and W (= O1) denote different structural sites (Henry et al. 2011). These sites can have different possible occupants:

$^{IX}X = Na^+, K^+, Ca^{2+}, Pb^{2+}, \square$ (vacancy),
$^{VI}Y = Fe^{2+}, Mg^{2+}, Mn^{2+}, Al^{3+}, Li^+, Fe^{3+}, Cr^{3+}, V^{3+}, Ti^{4+}, Zn^{2+}, Cu^{2+}, Ni^{2+}, ...$
$^{VI}Z = Al^{3+}, Fe^{3+}, Cr^{3+}, V^{3+}, Mg^{2+}, Fe^{2+}, ...$
$^{IV}T = Si^{4+}, Al^{3+}, B^{3+},$
$^{III}B = B^{3+},$
$^{III}V = OH^-, O^{2-},$
$^{III}W = OH^-, F^-, O^{2-}.$

Some of these constituents can be simultaneously present on two and even three structural sites, reflecting order-disorder phenomenon mainly between the octahedral Y- and Z-site occupants or oxygen and hydroxyl on the V and W sites. Substitutions among the heterovalent Y- and Z-site occupants are often

* E-mail: pieczka@agh.edu.pl. ORCID 0000-0002-2841-7313.

coupled with ion replacements at other structural sites, mainly at the X, V, and W. Four of the sites (Y, Z, V, W) form an octahedral cluster [$V_3Y_3Z_6W$] developed in the unit cell around (0, 0, 0), (2/3, 1/3/, 1/3), and (1/3, 2/3, 2/3), with a symmetry consistent with the $R3m$ space group. In consequence of these substitutions, the tourmaline supergroup comprises currently 35 valid mineral species accepted by the Commission on New Minerals, Nomenclature and Classification (CNMNC) of the International Mineralogical Association (IMA). They represent hydroxyl-, fluor- and oxy-species of X-vacant-, alkali-, and calcic tourmalines with typical octahedral occupants like Fe^{2+}, Mg^{2+}, Mn^{2+}, Al^{3+}, Li^+, Fe^{3+}, Cr^{3+}, and V^{3+} (Henry et al. 2011). Much less common are crystals highly enriched in atypical components like Pb (Sokolov and Martin 2009), Ti (Lottermoser and Plimer 1987; Vezzoni et al. 2018), Cu (Vereshchagin et al. 2013), Ni (Baksheev and Kudryavtseva 2004), Mn^{3+} (Bosi et al. 2017), Zn (Sokolov et al. 1988; Henry and Dutrow 1996; Ferreira et al. 2005; Pieczka et al. 2018), or K (Žáček et al. 2000; Lussier et al. 2016). The Zn-enriched tourmalines are represented mainly by fluor-elbaite, rarer elbaite, in which Zn^{2+}, beside typical Al^{3+} and Li^+, is one of the main octahedral Y-site occupants. Until quite lately, the most Zn-enriched tourmaline (3.83 wt% ZnO) was known from a rare-element-bearing pegmatite of Russia (Sokolov et al. 1988). However, recently Pieczka et al. (2018) described Zn-rich fluor-elbaite and elbaite containing up to 6.32 and 7.37 wt% ZnO, respectively, in a rare-element dike of the Julianna pegmatitic system, exposed during mining works in a migmatite-amphibolite quarry at Piława Górna, Lower Silesia, Poland (Szuszkiewicz et al. 2013). In the dike, these tourmalines, associated with Zn-enriched schorl and foitite (up to 2.45 wt% ZnO), formed a thin metasomatic zone around gahnite, changing progressively into typical, only slightly Zn-enriched, fluor-elbaite and elbaite. In the original paper, the occurrence and compositional relationships of the tourmalines were described in detail, as well as a Raman spectrum of Zn-rich fluor-elbaite was presented. Unfortunately, in Pieczka et al. (2018) the captions for Figures 9a and 9b presenting the Raman spectra of O–H stretching modes in Zn-rich fluor-elbaite and associated (Zn,Li)-bearing schorl in the range of 3400–3800 cm^{-1} were inadvertently switched, i.e., the caption b should be a and conversely, consistent with Figure 8 presenting both these spectra in the range of 50–4000 cm^{-1}.

Raman spectroscopy is a method commonly used in mineralogy for a quick identification of minerals because an extensive sample preparation is not necessary and, similarly to infrared spectroscopy, it is known as a non-destructive method giving fingerprint of a specific species. The great advantage of Raman spectroscopy is its capability to analyze areas as small as ~1 μm^2, which makes it useful in studies of highly heterogeneous materials, which require micrometer-scale spatial resolution. The acquisition area of the method is only somewhat smaller, but may be comparable with the acquisition area of the electron probe microanalysis–wavelength-dispersive (EPMA-WDS), at least an order of magnitude smaller than the crystal dimensions required by single-crystal X-ray diffraction as the basic method of structure recognition. This capability can make Raman spectroscopy a very useful and complementary tool in crystal-chemical and structural studies. Moreover, because ^VOH and ^WOH anions are bonded to different Y-site occupants as well as to Al at the Z site,

O–H stretching modes in Raman spectra of Li-bearing tourmalines contain critical crystal-chemical and structural information of the structural part with the greatest compositional variation. Therefore, in this paper, we analyze the possibility of a Raman spectroscopy application for a fast evaluation of crystal-chemical relationships in Li-bearing tourmalines, especially the quantitative estimation of the Y-site population and of the ^WOH amount. To present the possibilities of Raman spectroscopy, we discuss the crystal structure and explain in detail the Raman spectrum of this Zn-rich fluor-elbaite, especially focusing on O–H stretching vibrations in which our interpretation is in agreement with the structural and compositional results.

MATERIALS AND METHODS

Electron probe microanalysis (EPMA)

Electron probe microanalysis of Zn-rich fluor-elbaite in a zone around gahnite was performed at the Inter-Institute Analytical Complex for Minerals and Synthetic Substances at the University of Warsaw, Poland, using a Cameca SX 100 electron microprobe (CAMECA, Cedex, France). The analyses were made on a grinded, polished, and coated with carbon small fragment of the pegmatite mounted in 1-inch epoxy disk with the gahnite crystals overgrown by Zn-rich fluor-elbaite. The microprobe operated in WDS mode under the following conditions: accelerating voltage of 15 kV, beam current of 10 nA, beam diameter of 2 μm, peak count-time of 20 s, background time of 10 s. Standards (analytical lines, diffracting crystals, and mean detection limits in wt% element) were as follows: fluorophlogopite (F $K\alpha$, PC0, 0.12), albite (Na $K\alpha$, TAP, 0.03), diopside (Mg $K\alpha$, TAP, 0.02), (Si $K\alpha$, TAP, 0.03), and (Ca $K\alpha$, PET, 0.02), orthoclase (Al $K\alpha$, TAP, 0.03) and ($K\alpha$, PET, 0.02), rutile (Ti $K\alpha$, LPET, 0.02), rhodonite (Mn $K\alpha$, LIF, 0.09), hematite (Fe $K\alpha$, LIF, 0.08), V_2O_5 (V $K\alpha$, LIF, 0.06), Cr_2O_3 (Cr $K\alpha$, LPET, 0.02), and sphalerite (Zn $K\alpha$, LIF, 0.09). The raw data were reduced with the PAP routine of Pouchou and Pichoir (1991). The estimation of the Li_2O amounts from EPMA results on the basis of a multiple-regression equation of Pesquera et al. (2016) did not give positive result because the calculated Li_2O amount (in wt%) is distinctly ZnO dependent for higher ZnO contents (Pieczka et al. 2018). Therefore, we estimated the Li_2O and H_2O contents on the basis of the refined Y- and W-site scattering values. The atomic contents and chemical formula of the Zn-rich fluor-elbaite were normalized in relation to 14.5 (O,OH,F) anions pfu, i.e., 31 (O,OH,F) – 12 O – 4.5 O after assumption of 6 Si atoms per formula unit (apfu), 3 B atoms, total Fe as FeO, and Li_2O and H_2O amounts matching the calculated Li and OH contents during the formula calculation to the refined Y-site electron density, and the sum of Y-site occupants equal to 3 apfu. A small excess of Si above 6 apfu for the measured SiO_2 amount indicated at the applied normalization was considered as a small inaccuracy in the SiO_2 analysis [below 1.5 standard deviation (SD) of a single EPMA Si determination] or as an external admixture, for example of quartz micro-inclusions occurring in the Zn-rich fluor-elbaite zone. The EPMA results recalculated in such way presented in Table 1 correspond to spot analyses of Zn-rich fluor-elbaite, observed in one area of a zone around gahnite (Fig. 1). From this area, in which also micro-Raman spectra were collected (discussed in Pieczka et al. 2018), we extracted a small fragment of this tourmaline for the single-crystal X-ray diffraction investigation.

Crystal structure refinement (SREF)

The crystal structure of Zn-rich fluor-elbaite was refined at the Institut für Mineralogie und Kristallographie, Geozentrum, Universität Wien, Austria. As a first step, the quality of different tourmaline crystals was checked with a Bruker APEXII diffractometer equipped with a CCD area detector and an Incoatec Microfocus Source IμS (30 W, multilayer mirror, Mo$K\alpha$). The crystal with the best quality, 170 × 150 × 120 μm in size, was subsequently measured on this diffractometer. Single-crystal X-ray diffraction data, up to 80.52° 2θ, were collected at room temperature, integrated and corrected for Lorentz and polarization factors, with an absorption correction by evaluation of partial multiscans. The structure was refined with SHELXL97 (Sheldrick 1998) using scattering factors for neutral atoms and a tourmaline starting model from Ertl et al. (2010) (sample R6b). Refinement was performed with anisotropic displacement parameters for all non-hydrogen atoms. Supplemental Material[1] (CIF) provides crystal data and details of the structure refinement. The various site occupancies were refined according to well-known

TABLE 1. Chemical composition of Zn-rich fluor-elbaite from Piława Górna

| Component	9/1	18/8	20/9	8/4	average (wt%)		average (apfu)	+1sd (apfu)	+2sd (apfu)	+3sd (apfu)	RS (apfu)
SiO_2	36.96	36.10	36.06	37.08	36.55(47)	Si^{4+}	6.04(8)	6.04(8)	6.05(8)	6.05(8)	6.08(8)
Al_2O_3	36.64	35.70	35.75	36.98	36.27(56)	Al^{3+}	7.06(11)	7.06(11)	7.07(11)	7.08(11)	7.11(11)
FeO	2.45	2.37	2.42	1.92	2.29(22)	Fe^{2+}	0.32(3)	0.32(3)	0.32(3)	0.32(3)	0.32(3)
MnO	0.67	0.58	0.61	0.76	0.66(07)	Mn^{2+}	0.09(1)	0.09(1)	0.09(1)	0.09(1)	0.09(1)
ZnO	5.64	5.90	5.57	5.68	5.70(12)	Zn^{2+}	0.69(1)	0.70(1)	0.70(1)	0.70(1)	0.70(2)
CaO	0.07	0.09	0.08	0.10	0.08(01)	Ca^{2+}	0.01(0)	0.01(0)	0.01(0)	0.01(0)	0.01(0)
Na_2O	2.70	2.62	2.61	2.62	2.64(04)	Na^+	0.84(1)	0.85(1)	0.85(1)	0.85(1)	0.85(1)
F	1.35	1.18	1.24	1.19	1.24(07)	F^-	0.65(4)	0.65(4)	0.65(4)	0.65(4)	0.65(4)
$B_2O_{3(calc)}$					10.53	B^{3+}	3.00	3.00	3.00	3.00	3.00
$Li_2O_{(calc)}$					1.26	Li^+	0.84	0.83	0.82	0.81	0.78
$H_2O_{(calc)}$					2.96	OH^-	3.26	3.24	3.23	3.21	3.13
$-O=F_2$					-0.52	O^{2-}	27.09	27.11	27.12	27.14	27.22
Total					99.65						

Notes: RS = average EPMA analysis completed with Li_2O and H_2O amounts matched to the SREF measured Y-site scattering; +1sd, +2sd, and +3sd analyses = EPMA analysis completed with Li_2O and H_2O amounts matched to the SREF measured Y-site scattering +1sd, +2sd, or +3sd, respectively. EPMA analysis completed with Li_2O and H_2O amounts matched to the $^{V}OH_{Y_{Al}Z_{Al}Z_{Al}}/(^{V}OH_{Y_{ZZ}} + ^{W}OH_{Y_{YY}})$ parameter equal to 0.3558, designed from the deconvoluted Raman spectrum. For the +1sd, +2sd, +3sd, and RS analyses contents (in wt%) of the calculated components B_2O_3, Li_2O, and H_2O are equal to: 10.52, 10.50, 10.49, and 10.44 (B_2O_3); 1.25, 1.24, 1.22, and 1.16 (Li_2O); 2.94, 2.92, 2.90, and 2.82 (H_2O); totals 99.61, 99.56, 99.52, and 99.32, respectively.

characteristics of the tourmaline structure and considering the electron-probe analysis; this strategy appears sound with the resulting empirical formula being compatible with that determined from the EPMA results. Hence, the X-site occupancy was refined by using a Na scattering factor, the Y site with Zn and Li scattering factors, and the W site with F and O scattering factors, whereas the Si occupancy at the T site and the Al occupancy at the Z site were fixed at 1.00, typical for (Al,Li)-bearing tourmalines. A preliminary refinement, with O1 and O2 sites constrained to their positions of maximum site-symmetry, has shown relatively high U_{eq} values for these both oxygen sites. Following the findings of Burns et al. (1994), who reported high U_{eq} values for the O1 and O2 sites that indicate position disorder, the crystal structure was finally refined with both oxygen sites allowed to disorder with coordinates (x, x/2, z) and (x, y, z). The refinement converged at a $R1(F)$ value of 1.67%.

Raman spectroscopy

Raman spectra of Zn-rich fluor-elbaite were collected in backscattered geometry at the Faculty of Materials Science and Ceramics, AGH UST, Cracow, Poland, with a Horiba Labram HR spectrometer integrated with an Olympus BX 41 confocal microscope. The system was calibrated using the 520.7 cm^{-1} Raman band of Si. The spectra were recorded in the range of 50–4000 cm^{-1} using the 532 nm line of a solid-state Nd-YAG laser (10 mW) and 1800 grating, on randomly oriented surfaces of Zn-rich tourmaline in a fragment of the pegmatite mounted in epoxy resin that was used previously for EPMA and partly extracted for SREF studies. Prior to the Raman measurements, the carbon coating of the disk was removed. The Raman measurements were carried out by the accumulation of two scans with a precision of ±0.39 cm^{-1}, each with an acquisition time of 600 s

Figure 1. Backscattered-electron image (colors added) of zinc-rich fluor-elbaite and schorl from Piława Górna, Lower Silesia, southwestern Poland (enlargement of a part of Pieczka et al. 2018, Fig. 4d). The area analyzed with the electron microprobe, single-crystal X-ray diffraction, and Raman spectroscopy is enclosed by a red ellipse.
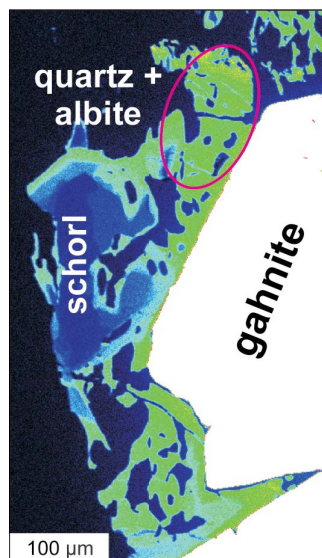
at the microscope magnification 100×; the minimum lateral and depth resolution ~1 μm, and an estimated analytical spot size of ~1 μm. Because all the spectra recorded on a small fragment of the tourmaline were very similar one to the other in the range of OH stretching vibrations (3400–3800 cm^{-1}), only one representative spectrum was resolved, the same that was presented and initially interpreted by Pieczka et al. (2018).

An initial resolution of the recorded spectrum was done in the range of 3400–3800 cm^{-1} applying the FITYK program for data processing and nonlinear curve fitting (Wojdyr 2010), after subtracting a linear background. To identify hidden bands, peak positions, full-widths at half maximum (FWHM), and integrated intensities were determined by fitting with pseudo-Voigt (PV) functions PV = $x \cdot$Lorentz + (1–x)·Gauss, with x varying in the range from 0 (0%) to 1 (100%), applying the Levenberg-Marquardt algorithm (Levenberg 1944; Marquardt 1963). Although good fits with $R^2 > 0.995$ to the empirical spectrum were easily achieved, the theoretical Y- and W-site occupants in these models differ to the occupants as determined by EPMA and SREF, probably due to different fractions of the Lorentzian and Gaussian components in the fitted component bands. Additionally, initial bands with small intensities very often have been eliminated during fitting by their addition to nearby more intense bands by increasing their Lorentzian component. Therefore, the final fitting was performed on an input model of component bands with Gaussian function shapes and application of the Levenberg-Marquardt fitting method. Spectral position, height, and FWHM of each anticipated band were matched in such a way to minimize the difference between the empirical spectrum and the theoretical spectrum designated as the sum of intensities of the anticipated bands, considering: (1) the fine structure of the spectrum and information on spectral positions and assignments of O–H stretching vibrations in Li-bearing tourmalines (Gonzalez-Carreño et al. 1988; Hoang et al. 2011; Skogby et al. 2012; Fantini et al. 2014; Watenphul et al. 2016a; Mercurio et al. 2018; Bronzova et al. 2019), and (2) the crystal-chemical data of the studied tourmaline making a possible explanation of the component bands by local ^{V}OH and ^{W}OH short-range arrangements. A weak band ~3450 cm^{-1} with a total intensity ~3.5–3.6% of the total spectrum (tested with various variants of the spectrum deconvolution) was related to a fluorescence band. The spectrum was slightly smoothed prior to the fitting procedure to better isolate the peak maxima, first of all for bands above 3600 cm^{-1} with very small intensities.

RESULTS AND DISCUSSION

Crystal structure

By using the refinement and the chemical data, the Zn-rich fluor-elbaite features the following average empirical formula: $^{X}(Na_{0.84}\square_{0.14}Ca_{0.01})_{\Sigma1.00}{}^{Y}(Al_{1.06}Li_{0.84}Zn_{0.69}Fe^{2+}_{0.32}Mn_{0.09})_{\Sigma3.00}$ $^{Z}Al_6(BO_3)_3(^{T}Si_6O_{18})^{V}(OH)_3{}^{W}(F_{0.65}OH_{0.26}O_{0.09})$. Its structure was refined with $R1$ value of 1.67% for 2304 reflections. The refined unit-cell parameters of the tourmaline are: $a = 15.921(1)$, $c = 7.127(1)$ Å, and $V = 1564.5(3)$ Å^3. In the refinement, the T, B, Z, and V sites were fixed with complete occupancies by Si, B, Al, and OH, respectively, in accordance with the average distances

and with many other Al-rich and Li-bearing tourmalines (e.g., Donnay and Barton 1972; Burns et al. 1994; Shtukenberg et al. 2007; Ertl et al. 2013). Although the T site in Al-rich, Li-bearing tourmalines may sometimes exhibit a small amount of tetrahedrally coordinated boron, the refined <T–O> mean distance of 1.6197(5) Å, is within one standard deviation identical with the <Si–O> bond length for tourmaline as given by MacDonald and Hawthorne (1995) and Bosi and Lucchesi (2007), which were estimated as 1.620 and 1.619(1) Å, respectively. This indicates that the T site of this tourmaline is filled exclusively by Si. This is also in agreement (within 1 SD) with the SiO_2 measured by EPMA [6.04(8) apfu; Table 1]. The B site is occupied only with boron, as the refined mean bond length <B–O> = 1.375(1) Å is compatible with a distance 1.374(2) Å evaluated by Bosi and Lucchesi (2007) for tourmalines with the site completely filled with B^{3+}. Similarly, the Z site features a <Z–O> distance of 1.9087(6) Å, also similar with such distances of other Li-bearing tourmalines where the Z site is completely filled by Al (e.g., Donnay and Barton 1972; Burns et al. 1994; Shtukenberg et al. 2007; Ertl et al. 2013). The refined X-site occupancy [<X–O> = 2.685(1) Å], corresponding to the presence at the site 0.821(6) Na apfu, agrees within 2 SD with the occupancy of the site by 0.85(1) Na + 0.01(0) Ca apfu [9.0(1) refined eps (electrons per site) vs. 9.6(2) eps calculated from the empirical formula]. The refined Y-site occupancy, $Zn_{0.477(1)}Li_{0.523(1)}$, indicating the refined site scattering of 15.87(3) eps corresponds to the estimated site population $(Al_{1.06}Li_{0.84}Zn_{0.69}Fe^{2+}_{0.32}Mn_{0.09})_{\Sigma 3.00}$, and the refined and calculated on the basis of Shannon's (1976) ionic radii <Y–O> mean bond lengths, 2.038(1) and 2.040 Å, respectively, are also the same. The occupancy of the V sites was fixed to 3 OH pfu with the refined V[= O(3)]–H(3) distance of 0.819 Å, showing a weak hydrogen bond with oxygen from O(5). The refined W-site occupancy, $F_{0.57(5)}O_{0.43(5)}$, is in good agreement with the microprobe data of F equal to 0.65(4) apfu [8.57(5) eps vs. 8.65(4) eps, respectively].

Micro-Raman spectroscopy

Although Raman and IR studies of tourmalines refer usually to the Si_6O_{18} rings, BO_3 groups and OH groups, all previous researchers agree that the O–H stretching vibrations in the range 3000–4000 cm^{-1}, carry the highest portion of crystal-chemical and structural information (Gonzalez-Carreño et al. 1988; Hoang et al. 2011; Skogby et al. 2012; Zhao et al. 2012; Fantini et al. 2014; Bosi et al. 2015, 2016; Berryman et al. 2016; Kutzschbach et al. 2016; Watenphul et al. 2016a; Mercurio et al. 2018; Bronzova et al. 2019). This is a result of the specific location of the ^VOH and ^WOH groups in the tourmaline structure because the ligands are bonded to the octahedrally coordinated occupants of the Y- and Z-sites, which are the two sites with the highest diversification in cation populations. Therefore, we agree with such statements as, for example, with Watenphul et al. (2016a) that "the stretching modes of the OH groups in the V and W sites are good candidates for establishing the functional relationship between Raman peak parameters and the crystal chemistry of tourmaline." Furthermore, it should be possible to use this relationship for a fast evaluation of the Y- and W-site populations for other Al-rich and Li-bearing tourmalines, when we are able to decode this relationship. Hence, we must consider

that the O–H stretching vibration range reflects quantitatively the chemical bonds of all OH groups from the V and W sites together with all bonded octahedral cations, and additionally, being under the influence of valence-varying X-site occupants (Ca^{2+}, Na^+, and K^+, and a formally zero-valence vacancy) and W-site occupants (OH^-/F^-, O^{2-}).

As our tourmaline is a fluor-elbaite, its crystal chemistry and structure is expected to be less complex: the Z site can be assumed to be occupied completely by Al, i.e., without a noticeable disordering of Y- and Z-site cations like Mg or Fe, and the V sites can be assumed to be completely occupied by OH, assumptions shown to be valid in many previous studies of Al-rich and Li-bearing tourmalines. The structure refinement results of the studied fluor-elbaite presented above are consistent with this structural model. This restricts our band interpretation to an analysis of local arrangements around the ^VOH and ^WOH sites that depend mainly on the Y-site occupancy. Such a model of interpretation of O–H stretching modes in Raman or IR spectra of tourmalines is applied commonly, for example, Gonzalez-Carreño et al. (1988), Hoang et al. (2011), Skogby et al. (2012), Zhao et al. (2012), Fantini et al. (2014), Bosi et al. (2015), Berryman et al. (2016), Kutzschbach et al. (2016), Mercurio et al. (2018), and Bronzova et al. (2019). Applying this model, we will show that Raman spectroscopy of an Al-rich and Li-bearing tourmaline together with a proper deconvolution of its spectrum can lead to Y- and W-site occupancies comparable with those derived from single-crystal X-ray diffraction.

Watenphul et al. (2016a) presented an alternative interpretation of the ^VOH stretching modes based on the site-symmetry analysis, which led to the assumption that H atoms of the ^VOH groups are related by rotation around the threefold axis and collectively participate in a single phonon mode. In consequence, the energy of the ^VO–H stretching band should be affected by local cation arrangements associated with all the three ^VOH groups bonded to all cations of the octahedral cluster, which schematically may be presented as $^V(OH)_3$-[YZZ–YZZ–YZZ]. This model was also used by Bosi et al. (2016) in studies of thermal stability of the octahedral clusters in dravite. In contrast, the model exploring individual local arrangements around each of the three ^VOH groups takes into account the influence of 1/3 portion of the octahedral cluster $[^VOH–YZ_2]_3$, which is developed around the threefold axis (the W site is omitted in the two schemes) modifying the energy of the ^VO–H stretching band in the single ^VOH group. Schematically it may be presented as ^VOH-[YZZ]. To explain why we finally decided to employ the short-range arrangement model for the interpretation of our tourmaline spectrum, we first will have to discuss the results of the deconvolution of the Zn-rich fluor-elbaite spectrum, consistent with the assumption of Watenphul et al. (2016a).

Figure 2a presents Raman spectrum of the Zn-rich fluor-elbaite in the range of O–H stretching modes (3400–3800 cm^{-1}). The spectrum has three intense peaks with the maxima at 3497, 3561, and 3597 cm^{-1}. Peaks with similar Raman shifts in the spectrum of elbaite (3494 ± 8, 3562 ± 4, and 3593 ± 4 cm^{-1}) were assigned by Watenphul et al. (2016a) to ^VO–H stretching modes related to the octahedral clusters: $^YLi^ZAl^ZAl$-$(^YAl^ZAl^ZAl)_2$, $(Y^{2+}^ZAl^ZAl)_2$-$^YAl^ZAl^ZAl$, and $(^YLi^ZAl^ZAl)_2$-$^YAl^ZAl^ZAl$, where Y^{2+} denotes the total of all divalent Y-site occupants

Figure 2. Deconvolution of the O–H vibration modes in Zn-rich fluor-elbaite with the model of Watenphul et al. (2016a). (**a**) Four ^{V}OH component bands. (**b**) Six ^{V}OH component bands (explanation in the text). Colors in the spectrum: gray = the measured spectrum, black = the smoothed spectrum, red = the fitted model, orange = a fluorescence band, blue = bands of ^{V}O–H vibrations, green = bands of ^{W}O–H vibrations.

(Y^{2+} = Fe^{2+} + Mn^{2+} + Zn^{2+} + Mg^{2+}). A visible asymmetry of the peak 3497 cm^{-1} centered at ~3475 cm^{-1} would be assigned to the Y^{2+Z}Al-($^YAl^ZAl^ZAl$)$_2$ cluster (Watenphul et al. 2016a; their Table 3, p.977). The deconvolution of the spectrum in the range of ^{V}O–H stretching modes into four component bands, as was suggested in the paper above, was done with a high R^2 = 99.95%, with pseudo-Voigt functions and in majority free values of peak center, height, and FWHM as presented in the upper part of Table 2. The fitted component bands 3481.6(9), 3498.9(4), 3560.3(0), and 3596.8(0) cm^{-1} locate within statistical Raman shift ranges as obtained by Watenphul et al. (2016a). However, the contents of ^{Y}Li, Y^{2+}, and ^{Y}Al calculated on the basis of the equation given by these authors (see p. 980) for the calculation of specific Y-site occupants on the basis of the band assignments, 0.59 Li, 1.04 Y^{2+}, and 1.37 Al apfu, differ significantly from those calculated on the basis of EPMA and SREF: 0.84, 1.10, and 1.06 apfu, respectively. The difference could be a result from the omission of two other possible [YZZ–YZZ–YZZ] clusters. These clusters are connected with ^{V}OH groups that must show up in a Raman spectrum of a Y^{2+}-bearing Li-tourmaline: $^YLi^ZAl^ZAl–Y^{2+Z}Al^ZAl–^YAl^ZAl^ZAl$ and ($Y^{2+Z}Al^ZAl$)$_3$. These clusters can be explained due to bond-valence constraints around the W site in the tourmaline structure (Hawthorne 1996, 2002, 2016; Bosi 2013), which allow seven variants of the [YYY] triplet, for which the W site can be occupied by OH$^-$/F$^-$ or O^{2-} at the simultaneous presence of OH$^-$ at the V site (Table 3). The first of the two arrangements cited above is especially important, because its frequency, compared to the cluster ($Y^{2+Z}Al^ZAl$)$_2$-$^YAl^ZAl^ZAl$, is commonly higher or at least equal, when the content of Y^{2+} is 2-times higher than the content of Li. Therefore, we also have tested a deconvolution of the spectrum into six ^{V}OH component bands, accepting that the arrangements ($^VOH–Y^{2+Z}Al^ZAl$)$_3$,

($^VOH–Y^{2+Z}Al^ZAl$)$_2$ × $^VOH–^YAl^ZAl^ZAl$, and $^VOH–^YLi^ZAl^ZAl$ × $^VOH–Y^{2+Z}Al^ZAl$ × $^VOH–^YAl^ZAl^ZAl$ could collectively correspond to the band observed at ~3561 cm^{-1}. Results of such a deconvolution that characterizes a similarly high R^2 are presented in Table 2 (lower part) and in Figure 2b. In this case, the integral intensities of the component bands centered at 3477.9(2), 3497.1(1), 3545(1), 3555.7, 3564.2(1), and 3596.3(0) cm^{-1} and their assignments indicate the presence of 0.93 Li, 0.80 Y^{2+},

TABLE 2. Deconvolution of O-H stretching bands in Zn-rich fluor-elbaite consistently with the model of Watenphul et al. (2016a)[a]

Raman shift (cm^{-1})	FWHM (cm^{-1})	Integral intensity (%)	Interpretation
3481.6(9)	30.0(6)	15.66	^VOH-$Y^{2+Z}Al^ZAl$ × ^VOH–($^YAl^ZAl^ZAl$)$_2$
3498.9(4)	25.7(3)	20.17	^VOH–$^YLi^ZAl^ZAl$ × ^VOH–($^YAl^ZAl^ZAl$)$_2$
3560.3(0)	28.4(1)	43.11	(^VOH-$Y^{2+Z}Al^ZAl$)$_2$ × ^VOH–$^YAl^ZAl^ZAl$
3596.8(0)	21.0(1)	18.65	(^VOH–$^YLi^ZAl^ZAl$)$_2$ × ^VOH–$^YAl^ZAl^ZAl$
3629.3(3)	8	0.28	^WOH-$Y^{2+Y}Al^YAl$···□
3642.0(8)	8	0.07	^WOH-$Y^{2+}Y^{2+Y}Al$···□
3672.0(3)	10.0(8)	0.40	^WOH-YYY···(□,Na)
3682.2(4)	10(1)	0.54	^WOH-YYY···Na
3713(1)	39(4)	1.12	^WOH-YYY···(Na,Ca)
3477.9(2)	26	11.65	^VOH-$Y^{2+Z}Al^ZAl$ × (^VOH–$^YAl^ZAl^ZAl$)$_2$
3497.1(1)	28.0(2)	26.94	^VOH–$^YLi^ZAl^ZAl$ × (^VOH–$^YAl^ZAl^ZAl$)$_2$
3545(1)	24(2)	3.46	(^VOH-$Y^{2+Z}Al^ZAl$)$_3$
3555.7	22	12.55	(^VOH-$Y^{2+Z}Al^ZAl$)$_2$ × ^VOH–$^YAl^ZAl^ZAl$
3564.2(1)	22	21.65	^VOH–$^YLi^ZAl^ZAl$ × ^VOH–$Y^{2+Z}Al^ZAl$ × ^VOH–$^YAl^ZAl^ZAl$
3596.3(0)	22.2(1)	21.05	(^VOH–$^YLi^ZAl^ZAl$)$_2$ × ^VOH–$^YAl^ZAl^ZAl$
3629.4(5)	8	0.27	^WOH-$Y^{2+Y}Al^YAl$···□
3641.8(4)	8	0.16	^WOH-$Y^{2+}Y^{2+Y}Al$···□
3670.8(4)	9(1)	0.33	^WOH-YYY···(□,Na)
3680(1)	16(2)	0.75	^WOH-YYY···Na
3713.1(7)	37	1.18	^WOH-YYY···(Na,Ca)

[a] Upper part presents the deconvolution into four component bands for ^{V}OH, lower part presents the deconvolution of the spectrum with two additional components (see explanation in the text); FWHM = full widths at half maximum. Data in parentheses are standard deviations. The lack of such data at peak positions or FWHM denotes that the parameters were fixed.

TABLE 3. Possible W-[YYY] short-range arrangements in tourmaline with ^{Z}Al and ^{V}OH

[YYY] arrangement	W		
	X = □	X = Na	X = Ca
[AlAlY^{2+}]	O		
[AlAlLi]	OH/F	OH/F^a or O	
[AlY^{2+}Y^{2+}]	OH/F	OH/F	
[AlY^{2+}Li]		OH/F	
[Y^{2+}Y^{2+}Y^{2+}]		OH/F	
[AlLiLi]		OH/F^a	
[Y^{2+}Y^{2+}Li]			OH/F^b

^{a} In elbaite and fluor-elbaite.
^{b} In Y^{2+}-bearing fluor-liddicoatite.

and 1.27 Al apfu, although the contents also differ to the EPMA + SREF results. The discrepancy among the EPMA + SREF contents and the contents estimated on the basis of the equation (directly related to the used interpretation model) is also visible in Figure 7 in the original paper of Watenphul et al. (2016a), where the deviations among the contents of Y-site occupants, evaluated by applying these two methods, are relatively distinct. In our opinion is this a serious problem of this model, particularly when the Y-site occupants represent a more complicated ternary system (Li$^+$, Y^{2+}, Al^{3+}).

The input model of Raman spectrum in the O–H stretching vibration range

Similarly to other researchers (Gonzalez-Carreño et al. 1988; Hoang et al. 2011; Skogby et al. 2012; Zhao et al. 2012; Fantini et al. 2014; Bosi et al. 2015; Berryman et al. 2016; Kutzschbach et al. 2016; Mercurio et al. 2018; Bronzova et al. 2019) we accept that Raman shifts of the ^{V}O–H stretching bands in tourmaline are dependent on the valence of one bonded Y-site occupant, in Al-rich and Li-bearing tourmalines varying from 3+ to 1+. Because each of the ^{V}OH groups is bonded to one Y and two Z cations and Z site is exclusively occupied by Al as is the case in Al-rich and Li-bearing tourmalines, the only possible arrangements of the [YZZ] triplet around the V site are ^{Y}Al^{Z}Al^{Z}Al, Y^{2+Z}Al^{Z}Al, and ^{Y}Li^{Z}Al^{Z}Al. The Y cations with different valences shift the electron density away from the ^{V}O–H bond proportionally to its own charge, and as a result, the ^{V}O–H bond length increases, but its strength decreases in accord with the sequence ^{Y}Li$^+\cdots^V$O–H through Y$^{2+}\cdots^V$O–H to ^{Y}Al$^{3+}\cdots^V$O–H. Consequently, ^{Y}Li, Y^{2+}, and ^{Y}Al^{3+} are assigned to bands with the observed maxima 3597, 3561, and 3497 cm^{-1}, respectively. Because in the tourmaline structure ^{V}OH groups occur with at least 75% abundance relative to the total content of hydroxyls [3^{V}OH + ^{W}(OH,F,O)], the resulting Raman bands have relatively high intensities. An exact observation of the spectrum in Figure 2 allows noticing asymmetry of all the peaks toward lower Raman shifts. Kutzschbach et al. (2016) observed such an effect for the Al-peak in synthetic olenite and interpreted it as a result of the presence of vacancies at the X site. We agree with this interpretation, because an alkali-vacant-type substitution of X$^+$ + Y^{2+} = ^{X}□$^{0+}$ + ^{Y}Al^{3+}, with Al^{3+} at the Y sites, needs a vacant X site. However, in such a case, we must accept that cations at the remaining two octahedral sites of the [YYY] triplet are also related to this empty X site. Therefore, we should expect for our tourmaline with occupation of the X-site (Na$_{0.84}$□$_{0.14}$Ca$_{0.01}$)$_{\Sigma 1}$ the presence of, at least, doubled bands for each absorption peaks previously assigned to the presence of ^{Y}Al^{3+}, Y^{2+}, and ^{Y}Li. In case of a highly diversified X-site

population, each of the ^{V}OH-^{Y}Al^{Z}Al^{Z}Al and ^{V}OH-^{Y}Li^{Z}Al^{Z}Al absorption peaks could be deconvoluted even into three bands, related to the presence of vacancy, Na or Ca at the X site, as can be assumed on the basis of the bond-valence constraints around the W site (Hawthorne 1996, 2002, 2016; Bosi 2013) and to the related V-site occupancies (Table 3). All the expectations we considered in an input model of component bands related to the ^{V}O–H stretching vibrations, assuming the presence of three components for the bands centered at 3497 and 3597 cm^{-1} (influenced by ^{X}□, ^{X}Na, and ^{X}Ca) and two components for the band centered at 3561 cm^{-1} (influenced only by □ and Na).

The ^{W}OH hydroxyls are bonded to three Y cations and influenced by the X-site occupant, for example, Gonzalez-Carreño et al. (1988), Berryman et al. (2016), and Bronzova et al. (2019). The presence of Al, Y^{2+}, and Li at the Y site of the studied Zn-rich fluor-elbaite results in 10 variants of the [YYY] triplet, from which only seven variants are allowed through bond-valence constraints around the W site (Hawthorne 1996, 2002, 2016; Bosi 2013) as presented in Table 3. It allows to expect that at a small proportion of ^{W}OH in the total OH content ($\leq 25\%$), the abundances of individual [YYY] arrangements and corresponding intensities of component bands should only be subordinate. Therefore, they only have a potential to modify the basic pattern of the spectrum produced essentially by ^{V}OH bands at lower Raman shift values. Because H$^+$ of the ^{W}OH group receives repulsion from the charge of the X cation, the ^{W}O–H length is the longest at a vacant X site, shorter when the X-site is occupied by Na, and the shortest for ^{X}Ca^{2+}, and is inversely proportional to the respective bond strengths. Therefore, in a tourmaline spectrum ^{W}O–H$\cdots^X$□ bands should occur at relatively low Raman shifts ~3600–3650 cm^{-1} (a weak band at ~3615 cm^{-1} is still assigned by us to ^{V}OH groups bonded to ^{Y}Li^{+Z}Al^{Z}Al$\cdots^X$Ca), ^{W}O–H$\cdots^X$Na around 3700 cm^{-1} (Hoang et al. 2011; Skogby et al. 2012; Fantini et al. 2014; Berryman et al. 2016; Watenphul et al. 2016a), and ^{W}OH-^{Y}Al^{Y}Li^{Y}Li$\cdots^X$Ca and ^{W}OH-Y^{2+}Y^{2+}Li$\cdots^X$Ca bands might be expected above to 3700–3750 cm^{-1}. Applying to the [YYY] arrangements the same reasoning as those used above for the [YZZ] triplets, it can be expected that the strongest effect of shifting the electron density away from the ^{W}O–H bond would take place for a ^{Y}AlY^{2+}Y^{2+} arrangement, and the weakest for the ^{Y}Al^{Y}Li^{Y}Li triplet. Consequently, the ^{W}O–H bond should be the weakest in case of the first-type triplet, and the strongest for the last. Summarizing, considering bond-valence constraints around the W site (Hawthorne 1996, 2002, 2016; Bosi 2013), the combination of ^{W}OH$\cdots$X and ^{W}OH$\cdots$[YYY] effects should result in a spectrum as maximum nine component bands (Table 3) with low intensities, totally $\leq 25\%$ of the whole spectrum, occurring in the spectral range of ~3600 to ~3800 cm^{-1}. In consequence, our input model for a deconvolution of the spectrum of Zn-rich and Ca-poor fluor-elbaite comprises eight component bands, related to ^{V}O–H stretching modes and nine component bands related to ^{W}O–H stretching modes, both modified by the Y-site occupants and influenced by ^{X}□, ^{X}Na, and ^{X}Ca.
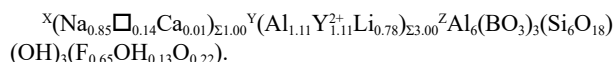
Fitting of the input model

Figure 3 and Table 4 present fitting results of the O–H stretching vibration range in the Zn-rich fluor-elbaite. The three asymmetrical peaks related to ^{V}O–H modes, centered at 3497,

TABLE 4. Deconvolution of O–H stretching vibration bands in Zn-rich fluor-elbaite according to the short-range arrangement model.

Raman shift (cm⁻¹)	FWHM (cm⁻¹)	Integral intensity (%)	Interpretation
3450	54		fluorescence
3478.1(3)	28.5	10.14	$^{V}OH–^{Y}Al^{Z}Al^{Z}Al...^{X}\square$
3498.1(1)	28.8(2)	24.96	$^{V}OH–^{Y}Al^{Z}Al^{Z}Al...^{X}Na$
3523.0(3)	10.8(8)	0.48	$^{V}OH–^{Y}Al^{Z}Al^{Z}Al...^{X}Ca$
3538.1(3)	26	5.55	$^{V}OH–Y^{2+Z}Al^{Z}Al...^{X}\square$
3561.2(1)	26.2	29.96	$^{V}OH–Y^{2+Z}Al^{Z}Al...^{X}Na$
3584.7(2)	11.7(5)	2.51	$^{V}OH–^{Y}Li^{Z}Al^{Z}Al...^{X}\square$
3597.5(1)	20.1(3)	21.17	$^{V}OH–^{Y}Li^{Z}Al^{Z}Al...^{X}Na$
3615.4(7)	10	0.29	$^{V}OH–^{Y}Li^{Z}Al^{Z}Al...^{X}Ca$
3625(1)	18	0.98	$^{W}OH–^{Y}Al^{Y}Al^{Y}Li...^{X}\square$
			$^{W}OH–^{Y}Al Y^{2+}Y^{2+}...^{X}\square$
3643(2)	25(3)	0.88	$^{W}OH–^{Y}Al^{Y}Al^{Y}Li...^{X}Na$
3671.9(4)	16	0.95	$^{W}OH–^{Y}Al Y^{2+}Y^{2+}...^{X}Na$
3683.5(6)	14	0.52	$^{W}OH–^{Y}Al Y^{2+}Y^{Y}Li...^{X}Na$
3697.8(8)	16	0.39	$^{W}OH–Y^{2+}Y^{2+}Y^{2+}...^{X}Na$
3715.5(6)	20	0.62	$^{W}OH–^{Y}Al^{Y}Li^{Y}Li...^{X}Na$
3737.6(8)	44.1	0.30	$^{W}OH–^{Y}Al^{Y}Li^{Y}Li...^{X}Ca$ (?)
3764.5(8)	45.1	0.30	$^{W}OH– Y^{2+}Y^{2+Y}Li...^{X}Ca$ (?)

Note: FWHM = full-width at half maximum. Data in parentheses are standard deviations. The lack of such data at peak position or FWHM denotes that the parameters were fixed.

3561, and 3597 cm⁻¹, were resolved into 3 + 2 + 3 component bands, respectively. We interpret them as $^{Y}Al^{Z}Al^{Z}Al$, $Y^{2+Z}Al^{Z}Al$, and $^{Y}Li^{Z}Al^{Z}Al$ arrangements modified by the presence of □ (the component band with the lowest Raman shift in each peak), Na⁺ or Ca²⁺ at the X site (the component band with the highest Raman shift in the first and third peak). Total intensities of the component bands corresponding to the presence of ^{Y}Al, Y^{2+}, or ^{Y}Li at the triplets $^{V}OH-[YZZ]$, i.e., $^{VOH}I_{YAlZAlZAl}$, $^{VOH}I_{Y2+ZAlZAl}$, and $^{VOH}I_{YLiZAlZAl}$, in relation to their sum, $^{VOH}I_{YZAlZAl}$, give shares of the Y constituents (Al, Y^{2+}, and Li) in the Y-site occupancy: ~37.4, 37.4, and 25.2%, respectively, which corresponds to the [YYY] triplet $(Al_{1.12}Y^{2+}_{1.12}Li_{0.76})_{\Sigma3}$. Furthermore, the ratio of total intensity
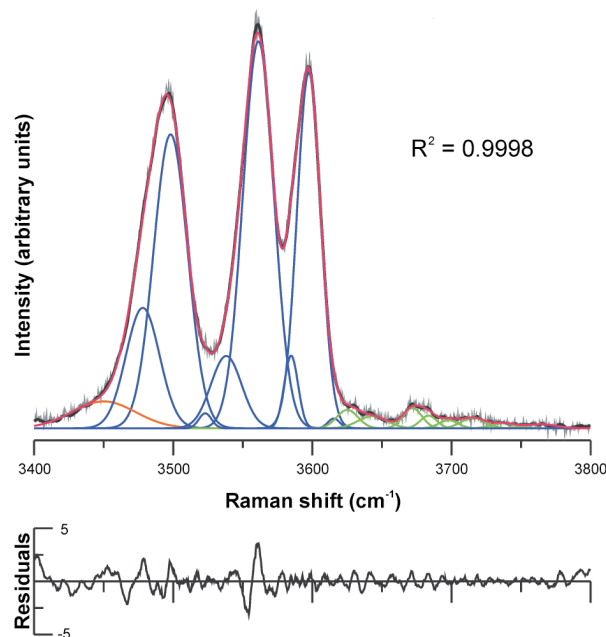
FIGURE 3. Deconvolution of the O–H vibration modes in Zn-rich fluor-elbaite with the short-range arrangement model. Colors as in Figure 2.

of the ^{V}OH bands, $^{VOH}I_{YZAlZAl}$, in relation to the total intensity of the ^{V}OH and ^{W}OH bands, $^{VOH}I_{YZAlZAl} + ^{WOH}I_{YYY}$, allows estimating an approximate $^{W}OH_{Raman}$ content from the equation: $^{W}OH = [3 \times (^{VOH}I_{YZAlZAl} + ^{WOH}I_{YYY})/^{VOH}I_{YZAlZAl} – 3]$ (apfu). For the studied fluor-elbaite the ^{W}OH content evaluated in such a way is ~0.16 apfu. The contents of 1.12 ^{Y}Al, 1.12 Y^{2+}, 0.76 ^{Y}Li apfu and 0.16 ^{W}OH groups pfu, estimated directly from the Raman spectrum of the fluor-elbaite after the deconvolution of the O–H stretching vibration range, correspond well to the EPMA + SREF results: 1.06 Al, 1.10 Y^{2+}, 0.84 Li, and 0.26 OH apfu. As a result, the output model of component bands in the OH stretching vibration range of the fluor-elbaite ascribes its empirical spectrum with a R^2 value of 0.9998, better than in the case of the previously discussed model of Watenphul et al. (2016a).
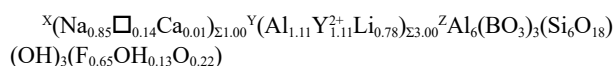
A deconvolution of the spectrum also gives an opportunity to use one of several quantitative parameters possible to evaluation in the calculation of the crystal-chemical formula, similarly as it was done, for example, for Li. Lithium cannot be analyzed by conventional microprobe, but evaluated on the basis of the EPMA results and the Y-site scattering from SREF. The introduction of such a parameter into the procedure of the formula calculation gives the opportunity to evaluate ^{Y}Li and ^{W}OH by matching of such Li₂O and H₂O amounts (in wt%) to obtain the value of the parameter matched to the value evaluated from the spectrum deconvolution. As the most suitable parameter we determined the content of the ^{V}OH-$^{Y}Al^{Z}Al^{Z}Al$ component bands in the total spectrum, i.e., the ratio $^{VOH}I_{YAlZAlZAl}/(^{VOH}I_{YZZ} + ^{WOH}I_{YYY})$. This is due to the only small superposition of the ^{V}OH-$^{Y}Al^{Z}Al^{Z}Al$ component bands, influenced by $^{X}(\square,Na,Ca)$ with the remaining part of the spectrum, which gives the opportunity to evaluate the parameter with a relatively high accuracy. The crystal-chemical formula calculated in such a way (only on basis of the EPMA and RS results) for the studied fluor-elbaite (Table 1) is as follows:

$$^{X}(Na_{0.85}\square_{0.14}Ca_{0.01})_{\Sigma1.00}{}^{Y}(Al_{1.11}Y^{2+}_{1.11}Li_{0.78})_{\Sigma3.00}{}^{Z}Al_{6}(BO_{3})_{3}(Si_{6}O_{18})(OH)_{3}(F_{0.65}OH_{0.13}O_{0.22}).$$

It differs from the EPMA + SREF formula by +0.05 Al, +0.01 Y^{2+}, and –0.06 Li apfu.

IMPLICATIONS

The empirical EPMA and SREF formula of the studied Zn-rich fluor-elbaite is $^{X}(Na_{0.85}\square_{0.14}Ca_{0.01})_{\Sigma1.00}{}^{Y}(Al_{1.06}Li_{0.84}Zn_{0.69}Fe^{2+}_{0.32}Mn_{0.09})_{\Sigma3.00}{}^{Z}Al_{6}(BO_{3})_{3}(Si_{6}O_{18})(OH)_{3}(F_{0.65}OH_{0.26}O_{0.09})$. Our interpretation of the RS of the tourmaline in the range of O–H stretching modes, 3400–3800 cm⁻¹, indicates the presence of 1.12 Al, 1.12 Y^{2+}, and 0.76 Li apfu in the [YYY] triplet bonded to three ^{V}OH groups, and with OH, F, and O that occupy the W site. The ^{W}OH content deduced on the basis of the deconvolution of the spectrum is ~0.16 apfu, which leads to the W-site occupation $(F_{0.65}O_{0.19}OH_{0.16})_{\Sigma1}$. Applying the ratio $^{VOH}I_{YAlZAlZAl}/(^{VOH}I_{YZZ} + ^{WOH}I_{YYY})$, which reflects the contribution of ^{V}OH groups bonded to ^{Y}Al in relation to the total content of ^{V+W}OH groups, as an additional criterion in the formula calculation allows it to recalculate as

$$^{X}(Na_{0.85}\square_{0.14}Ca_{0.01})_{\Sigma1.00}{}^{Y}(Al_{1.11}Y^{2+}_{1.11}Li_{0.78})_{\Sigma3.00}{}^{Z}Al_{6}(BO_{3})_{3}(Si_{6}O_{18})(OH)_{3}(F_{0.65}OH_{0.13}O_{0.22})$$

where Y^{2+} = Zn + Fe + Mn, based only on electron microprobe and Raman spectroscopy results. The <Y–O> mean bond length calculated on the basis of the formula, 2.036 Å, as well as electron densities at the X, Y, and W sites, 9.6, 16.1, and 8.7 eps, respectively, agree well with the refined values (within ~2 SD SREF and EPMA results). Taking into account that in the applied methods (SREF, RS) the crystal-chemical and structural information were collected from volumes of the investigated crystal having different dimensions (i.e., ~1 μm^3 in RS vs. several cubic micrometers in EPMA compared to a significantly larger volume of ~3 × 10^6 μm^3 for the single-crystal X-ray diffraction) the accordance of both formulas in the order of +0.05 Al, +0.01 Y^{2+}, and –0.06 Li apfu, i.e., within 1 SD of the microprobe Al and Y^{2+} determinations, is an excellent agreement. Compared to the results of the deconvolution and interpretation of the spectrum, as was suggested by Watenphul et al. (2016a), +0.31 Al, –0.06 Y^{2+}, –0.25 Li apfu (deconvolution of the spectrum into 4 ^{Z}OH component bands), or +0.21 Al, –0.30 Y^{2+}, +0.09 Li apfu, (deconvolution into 6 ^{Z}OH component bands), our new proposed method gives results in better agreement with the EPMA and SREF results. Considering the standard deviations of the refined parameters (including site scattering) of the structure refinement, our (EPMA + RS)-evaluated formula actually seems to be very close to the calculated Y-site occupants (based on the EPMA + SREF results). Assuming Y-site scattering errors in the range of +1 to +3 SD, the differences between the (EPMA + RS)-evaluated Y-site contents (Al, Y^{2+}, Li) and those calculated from EPMA + SREF differ only by ±0.01 apfu per 1 SD at maximum (Table 1).

The presented results are the first documented case with the application of RS for the evaluation of the chemistry of a Li-bearing tourmaline. Up until now, only Watenphul et al. (2016b) attempted to apply RS to the discrimination of tourmaline species, which they showed was useful for discrimination of Mg- and Fe-dominant tourmaline species. Our presented method needs subsequent investigations for Al-rich and Li-bearing tourmalines representing other mineral species (elbaite, fluor-elbaite, fluor-liddicoatite, rossmanite, darrellhenryite), which additionally could validate it and should allow to obtain the influence of the orientation to the crystal faces and the precision of the Li and OH evaluation and ^{W}OH band assignments. More research about that is in progress. However, it seems that RS can be a very important tool in the achievement of crystal-chemical and structural information from ultra-small portions of a crystal, even smaller than needed for a single-crystal X-ray diffraction. Generally, it should not be surprising, because it is obvious that single-crystal X-ray diffraction and Raman spectroscopy present two different patterns of the same crystal structure and code the same crystal chemical and structural information, but in a different way. A crystal-structure refinement uses the intensities and positions of X-ray diffraction reflections, while Raman spectroscopy uses intensities and positions of absorption bands.

The determination of Li (Li$_2$O) in Li-tourmalines is still problematic. Rinaldi and Llovet (2015) stated that a new wavelength-dispersive (WDS) soft X-ray emission spectrometer (SXES) introduced by one of the two main EPMA equipment manufacturers opens a whole new perspective for the analysis of light elements (including Li) and low-energy lines of other elements in the nearest future. However, because Li can still not be analyzed by conventional EPMA instruments, for large and homogeneous crystals, this difficulty can only be overcome by a direct analysis of Li, for example, with AAS or LA-ICP-MS. These methods cannot be used for very small crystals, which show a complex zonation within a distance of a few micrometers. Tempesta and Agrosì (2016) studied the chemistry of red beryls (including Li) with approximately 10 μm spot sizes by using laser induced breakdown spectroscopy (LIBS), however, although this method is fast and only minimally destructive, it works without standards but yields quantitative results very close to those obtained with conventional techniques. Although the Li amount can be approximately evaluated on the basis of single-crystal X-ray diffraction, this method, currently mainly available at departments/faculties of chemistry, is not always accessible for mineralogists and cannot be applied routinely. To solve this problem, Pesquera et al. (2016) derived a statistical equation allowing the calculation of Li$_2$O content in weight percents from the amounts of main oxide components of Li-bearing tourmalines such as SiO$_2$, Al$_2$O$_3$, total Fe as FeO, and MnO. However, as shown by Pieczka et al. (2018), this method does not work well if a tourmaline is enriched by an atypical component, for example ZnO and even CaO, which are often present as important constituents in Al-rich, Li-bearing tourmalines. In this light, our presented method, providing comparable Li contents, estimated by the solution of O–H stretching vibration modes of a Raman spectrum of Li-tourmaline, can be applied relatively easily and quickly compared to single-crystal X-ray diffraction refinements. All the previous remarks also refer to the quantitative evaluation of OH$_{total}$ (H$_2$O), another important component, which is usually not analyzed and only calculated on basis of an assumed tourmaline stoichiometry. Raman spectroscopy gives an opportunity to determine the relatively exact amount of OH, although the V sites must be assumed the be fully occupied by OH. Hence, the amount of ^{W}OH can be determined as an excess above three anions per formula unit. We believe that with the EPMA-WDS chemical analysis and with Raman spectroscopy, it is possible to receive the correct crystal-chemical and structural formula of an Al-rich and Li-bearing tourmaline in a relatively short time without the necessity of comprehensive structural studies by single-crystal X-ray diffraction.

REFERENCES CITED

Baksheev, I.A., and Kudryavtseva, O.E. (2004) Nickeloan tourmaline from the Berezovskoe gold deposit, Middle Urals, Russia. Canadian Mineralogist, 42, 1065–1078.

Berryman, E.J., Wunder, B., Ertl, A., Koch-Müller, M., Rhede, D., Scheidl, K., Giester, G., and Heinrich, W. (2016) Influence of the X-site composition on tourmaline's crystal structure: Investigation of synthetic K-dravite, dravite, oxy-uvite, and magnesio-foitite using SREF and Raman spectroscopy. Physics and Chemistry of Minerals, 43, 83–102.

Bosi, F. (2013) Bond-valence constraints around the O1 site of tourmaline. Mineralogical Magazine, 77, 343–351.

Bosi, F., and Lucchesi, S. (2007) Crystal chemical relationships in the tourmaline group: Structural constraints on chemical variability. American Mineralogist, 92, 1054–1063.

Bosi, F., Skogby, H., Lazor, P., and Reznitskii, L. (2015) Atomic arrangements around the O3 site in Al- and Cr-rich oxy-tourmalines: a combined EMP, SREF, FTIR and Raman study. Physics and Chemistry of Minerals, 42, 441–453.

Bosi, F., Skogby, H., and Balić-Žunić, T. (2016) Thermal stability of extended clusters in dravite: A combined EMP, SREF and FTIR study. Physics and Chemistry of Minerals, 43, 395–407.

Bosi, F., Cámara, F., Ciriotti, M.E., Hålenius, U., Reznitskii, L., and Stagno, V. (2017) Crystal-chemical relations and classification problems of tourmalines belonging to the oxy-schorl–oxy-dravite–bosiite–povondraite series. European Journal of Mineralogy, 29, 445–455.

Bronzova, Y., Babushkina, M., Frank-Kamenetskaya, O., Vereshchagin, O., Rozhdestvenskaya, I., and Zolotarev, A. (2019) Short-range order in Li-Al tourmalines: IR spectroscopy, X-ray single crystal diffraction analysis and bond valence theory approach. Physics and Chemistry of Minerals, 46, 815–825.

Burns, P.C., MacDonald, D.J., and Hawthorne, F.C. (1994) The crystal chemistry of manganese-bearing elbaite. Canadian Mineralogist, 32, 31–41.

Donnay, G., and Barton, R. Jr. (1972) Refinement of the crystal structure of elbaite and the mechanism of tourmaline solid solution. TMPM Tschermaks Mineralogische und Petrographische Mitteilungen, 18, 273–286.

Ertl, A., Marschall, H.R., Giester, G., Henry, D.J., Schertl, H.-P., Ntaflos, T., Luvizotto, G.L., Nasdala, L., and Tillmanns, E. (2010) Metamorphic ultra high-pressure tourmalines: Structure, chemistry, and correlations to PT conditions. American Mineralogist, 95, 1–10.

Ertl, A., Giester, G., Schüssler, U., Brätz, H., Okrusch, M., Tillmanns, E., and Bank, H. (2013) Cu- and Mn-bearing tourmalines from Brazil and Mozambique: Crystal structures, chemistry and correlations. Mineralogy and Petrology, 107, 265–279.

Fantini, C., Tavares, M.C., Krambrock, K., Moreira, R.L., and Righi, A. (2014) Raman and infrared study of hydroxyl sites in natural uvite, fluor-uvite, magnesio-foitite, dravite and elbaite tourmalines. Physics and Chemistry of Minerals, 41, 247–254.

Ferreira, A.C.M., Ferreira, V.P., Soares, D.R., and Vilarroel-Leo, H.S. (2005) Chemical and mineralogical characterization of elbaite from the Alto Quixaba pegmatite, Seridó Province, NE Brazil. Anais da Academia Brasileira de Ciências, 77, 729–743.

Gonzalez-Carreño, T., Fernandez, M., and Sanz, J. (1988) Infrared and electron microprobe analysis of tourmalines. Physics and Chemistry of Minerals, 15, 452–460.

Hawthorne, F.C. (1996) Structural mechanisms for light-element variations in tourmaline. Canadian Mineralogist, 34, 123–132.

——— (2002) Bond-valence constraints on the chemical composition of tourmaline. Canadian Mineralogist, 40, 789–797.

——— (2016) Short-range atomic arrangements in minerals. I: The minerals of the amphibole, tourmaline and pyroxene supergroups. European Journal of Mineralogy, 28, 513–536.

Henry, D.J., and Dutrow, B.L. (1996) Metamorphic tourmaline and its petrologic applications. Reviews in Mineralogy and Geochemistry, 33, 503–557.

Henry, D.J., Novák, M., Hawthorne, F.C., Ertl, A., Dutrow, B.L., Uher, P., and Pezzotta, F. (2011) Nomenclature of the tourmaline-supergroup minerals. American Mineralogist, 96, 895–913.

Hoang, L.H., Hien, N.T.M., Chen, X.B., Minh, N.V., and Yang, I.-S. (2011) Raman spectroscopic study of various types of tourmalines. Journal of Raman Spectroscopy, 42, 1443–1446.

Kutzschbach, M., Wunder, B., Rhede, D., Koch-Müller, M., Ertl, A., Giester, G., Heinrich, W., and Franz, G. (2016) Tetrahedral boron in natural and synthetic HP/UPH tourmaline: Evidence from Raman spectroscopy, EMPA, and sinfle-crystal XRD. American Mineralogist, 101, 93–104.

Levenberg, K. (1944) A method for the solution of certain non-linear problems in least squares. Quarterly of Applied Mathematics, 2, 164–168.

Lottermoser, B.G., and Plimer, I.R. (1987) (1987) Chemical variation in tourmalines, Umberatana, South Australia. Neues Jahrbuch für Mineralogie Monatshefte, 7, 314–326.

Lussier, A., Ball, N.A., Hawthorne, F.C., Henry, D.J., Shimizu, R., Ogasawara, Y., and Ota, T. (2016) Maruyamaite, K(MgAl₂)(Al₅Mg)Si₆O₁₈(BO₃)₃(OH)₃O, a potassium-dominant tourmaline from the ultrahigh-pressure Kokchetav massif, northern Kazakhstan: Description and crystal structure. American Mineralogist, 101, 355-361.

MacDonald, D.J., and Hawthorne, F.C. (1995) The crystal chemistry of Si ↔ Al substitution in tourmaline. Canadian Mineralogist, 33, 849–858.

Marquardt, D. (1963) An algorithm for least-squares estimation of nonlinear parameters. SIAM Journal on Applied Mathematics, 11, 431–441.

Mercurio, M., Rossi, M., Izzo, F., Cappelletti, P., Germinario, C., Grifa, C., Petrelli, M., Vergara, A., and Langella, A. (2018) The characterization of natural gemstones using non-invasive FT-IR spectroscopy: New data on tourmalines. Talanta, 178, 147–159.

Pesquera, A., Gil-Crespo, P.P., Torres-Ruiz, F., Torres-Ruiz, J., and Roda-Robles, E. (2016) A multiple regression method for estimating Li in tourmaline from electron microprobe analyses. Mineralogical Magazine, 80, 1129–1133.

Pieczka, A., Gołębiowska, B., Jeleń, P., Włodek, A., Szełęg, E., and Szuszkiewicz, A. (2018) Towards Zn-dominant tourmaline: a case of Zn-rich fluor-elbaite and elbaite from the Julianna system at Piława Górna, Lower Silesia, SW Poland. Minerals, 8, 126.

Pouchou, J.-L., and Pichoir, F. (1991) Quantitative analysis of homogeneous or stratified microvolumes applying the model "PAP". In K.F.J. Heinrich and D.E. Newbury, Eds., Electron probe quantitation. Plenum Press, pp. 3l–75.

Rinaldi, R., and Llovet, X. (2015) Electron probe microanalysis: A review of the past, present, and future. Microscopy and Microanalysis, 21, 1053–1069.

Shannon, R.D. (1976) Revised effective ionic radii and systematic studies of interatomic distances in halides and chalcogenides. Acta Crystallographica, A32, 751–767.

Sheldrick, G.M. (1998) SHELXL97, Release 97-2. Program for crystal structure refinement. University of Göttingen, Germany.

Shtukenberg, A., Rozhdestvenskaya, I., Frank-Kamenetskaya, O., Bronzova, J., Euler, H., Kirfel, A., Bannova, I., and Zolotarev, A. (2007) Symmetry and crystal structure of biaxial elbaite-liddicoatite tourmaline from the Transbaikalia region, Russia. American Mineralogist, 92, 675–686.

Skogby, H., Bosi, F., and Lazor, P. (2012) Short-range order in tourmaline: A vibrational spectroscopic approach to elbaite. Physics and Chemistry of Minerals, 39, 811–816.

Sokolov, M., and Martin, R.F. (2009) A Pb-dominant member of the tourmaline group, Minh Tien granitic pegmatite, Luc Yen District, Vietnam. Estudos Geológicos, 19, 352–353.

Sokolov, P.B., Gorskaya, M.G., and Kretser, Yu.L. (1988) Zinc-bearing tourmalines from rare-metal pegmatites. Zapiski Vsesoyuznogo Mineralogicheskogo Obshchestva, 117, 70–74 (in Russian).

Szuszkiewicz, A., Szełęg, E., Pieczka, A., Ilnicki, S., Nejbert, K., Turniak, K., Banach, M., Łodziński, M., Różniak, R., and Michałowski, P. (2013) The Julianna pegmatite vein system at the Piława Górna mine, Góry Sowie Block, SW Poland – preliminary data on geology and descriptive mineralogy. Geological Quarterly, 57, 467–484.

Tempesta, G., and Agrosì, G. (2016) Standardless, minimally destructive chemical analysis of red beryls by means of Laser Induced Breakdown Spectroscopy. European Journal of Mineralogy, 28, 571–580.

Van Hinsberg, V.J., Henry, D.J., and Dutrow, B.L. (2011) Tourmaline as a petrologic forensic mineral: A unique recorder of its geologic past. Elements, 7, 327–332.

Vereshchagin, O.S., Rozhdestvenskaya, I.V., Frank-Kamenetskaya, O.V., Zolotarev, A.A., and Mashkovtsev, R.I. (2013) Crystal chemistry of Cu-bearing tourmalines. American Mineralogist, 98, 1610–1616.

Vezzoni, S., Biagioni, C., D'Orazio, M., Pieruccioni, D., Galanti, Y., Petrelli, M., and Molli, G. (2018) Evidence of Permian magmatism in the Alpi Apuane metamorphic complex (Northern Apennines, Italy): New hints for the geological evolution of the basement of the Adria plate. Lithos, 318-319, 104–123.

Watenphul, A., Burgdorf, M., Schlüter, J., Horn, I., Malcherek, T., and Mihailova, B. (2016a) Exploring the potential of Raman spectroscopy for crystallochemical analyses of complex hydrous silicates: II. Tourmalines. American Mineralogist, 101, 970–985.

Watenphul, A., Schlüter, J., Bosi, F., Skogby, H., Malcherek, T., and Mihailova, B. (2016b) Influence of the octahedral cationic-site occupancies on the framework vibrations of Li-free tourmalines, with implications for estimating temperature and oxygen fugacity in host rocks. American Mineralogist, 101, 2554–2563.

Wojdyr, M. (2010) Fityk, a general-purpose peak fitting program. Journal of Applied Crystallography, 43, 1126–1128.

Zhao, C., Liao, L., Xia, Z., and Sun, X. (2012) Temperature-dependent Raman and infrared spectroscopy study on iron-magnesium tourmalines with different Fe content. Vibrational Spectroscopy, 62, 28–34.

Žáček, V., Frýda, J., Petrov, A., and Hyršl, J. (2000) Tourmalines of the povondraite–(oxy)dravite series from the cap rock of meta-evaporite in Alto Chapare, Cochabamba, Bolivia. Journal of the Czech Geological Society, 45, 3–12.

Endnote:

[1]Deposit item AM-20-117360, CIF. Deposit items are free to all readers and found on the MSA website, via the specific issue's Table of Contents (go to http://www.minsocam.org/MSA/AmMin/TOC/2020/Nov2020_data/Nov2020_data.html).